

Recessive *LAMC3* mutations cause malformations of occipital cortical development

Tanyeri Barak^{1-3,18}, Kenneth Y Kwan^{2,4,18}, Angeliki Louvi^{1,2}, Veysi Demirbilek⁵, Serap Saygi⁶, Beyhan Tüysüz⁷, Murim Choi³, Hüseyin Boyacı^{8,9}, Katja Doerschner^{8,9}, Ying Zhu^{2,4}, Hande Kaymakçalan¹⁰, Saliha Yılmaz¹⁻³, Mehmet Bakırcioğlu¹⁻³, Ahmet Okay Çağlayan¹⁻³, Ali Kemal Öztürk¹⁻³, Katsuhito Yasuno¹⁻³, William J Brunken^{11,12}, Ergin Atalar⁹, Cengiz Yalçınkaya⁵, Alp Dinçer¹³, Richard A Bronen^{1,14}, Shrikant Mane^{3,15}, Tayfun Özçelik¹⁶, Richard P Lifton^{3,17}, Nenad Šestan^{2,4}, Kaya Bilgüvar¹⁻³ & Murat Günel¹⁻³

The biological basis for regional and inter-species differences in cerebral cortical morphology is poorly understood. We focused on consanguineous Turkish families with a single affected member with complex bilateral occipital cortical gyration abnormalities. By using whole-exome sequencing, we initially identified a homozygous 2-bp deletion in *LAMC3*, the laminin $\gamma 3$ gene, leading to an immediate premature termination codon. In two other affected individuals with nearly identical phenotypes, we identified a homozygous nonsense mutation and a compound heterozygous mutation. In human but not mouse fetal brain, *LAMC3* is enriched in postmitotic cortical plate neurons, localizing primarily to the somatodendritic compartment. *LAMC3* expression peaks between late gestation and late infancy, paralleling the expression of molecules that are important in dendritogenesis and synapse formation. The discovery of the molecular basis of this unusual occipital malformation furthers our understanding of the complex biology underlying the formation of cortical gyrations.

Extensive and stereotypic gyrations (convolutions) of the cerebral cortex are striking features of the human brain^{1,2}. The cerebral cortex develops through a series of highly coordinated phases including proliferation of neural progenitors, migration of postmitotic cells from the germinal matrix to the newly forming cortex and organization of the mature cortical cytoarchitecture. Among these processes, the biological basis for the formation of cortical convolutions has been the subject of much debate³⁻⁷. The study of malformations of

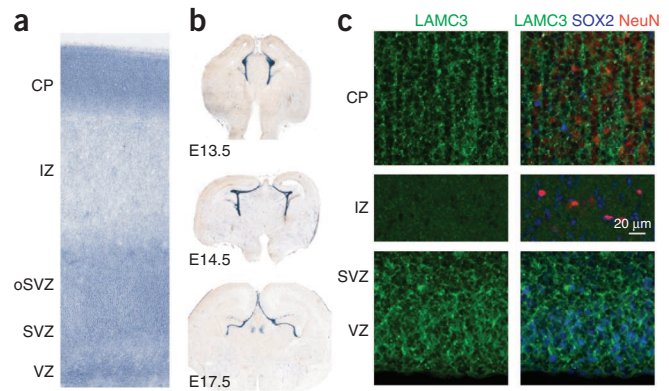
cortical development (MCD) that interfere with the proper formation of the typical cortical gyration pattern in humans provides a unique opportunity to understand this elegant process. We applied whole-exome capture and sequencing to the study of consanguineous, single-affected-member Turkish kindreds with malformations of occipital cortex gyration, notably characterized by the presence of both pachygyria and polymicrogyria^{8,9}, entities traditionally thought to arise from different pathogenic mechanisms reflecting abnormalities in neuronal migration and cortical organization, respectively¹⁰.

The first index case, designated NG 49-1 (Fig. 1a, Supplementary Fig. 1 and Supplementary Note), presented to medical attention with absence seizures and mild developmental delay during early childhood. Magnetic resonance imaging (MRI) revealed bilateral occipital pachygyria mainly localizing to the lateral surface, characterized by smoothing of the occipital cortices with loss of secondary and tertiary gyri, and polymicrogyric areas, characterized by the formation of numerous small gyri at the junction of the parieto-occipital lobes (Fig. 1b-f and Supplementary Videos 1 and 2). Following genome-wide genotyping, which confirmed consanguinity with an inbreeding coefficient of 5.77, and determination of homozygous genomic segments (>2.5 cM each) (Supplementary Table 1), we performed whole-exome capture and sequencing with high sensitivity and specificity using NimbleGen liquid-phase arrays and the Illumina Genome Analyzer-IIx instrument as described previously¹¹ (Supplementary Tables 2 and 3). By focusing on the homozygous intervals (Supplementary Table 4), we identified a homozygous 2-bp deletion in *LAMC3* (*Laminin $\gamma 3$*), which is located on chromosome 9; this mutation is inferred to result

¹Department of Neurosurgery, Yale School of Medicine, New Haven, Connecticut, USA. ²Department of Neurobiology, Yale School of Medicine, New Haven, Connecticut, USA. ³Department of Genetics, Center for Human Genetics and Genomics and Program on Neurogenetics, Yale School of Medicine, New Haven, Connecticut, USA. ⁴Kavli Institute for Neuroscience, Yale School of Medicine, New Haven, Connecticut, USA. ⁵Division of Child Neurology, Department of Neurology, Istanbul University Cerrahpasa Faculty of Medicine, Istanbul, Turkey. ⁶Department of Neurology, Hacettepe University School of Medicine, Ankara, Turkey. ⁷Division of Genetics, Department of Pediatrics, Istanbul University Cerrahpasa Faculty of Medicine, Istanbul, Turkey. ⁸Department of Psychology, Bilkent University, Ankara, Turkey. ⁹National Magnetic Resonance Research Center, Bilkent University, Ankara, Turkey. ¹⁰Faculty of Arts and Sciences, Bahcesehir University, Istanbul, Turkey. ¹¹Department of Cell Biology, State University of New York (SUNY) Downstate Medical Center, Brooklyn, New York, USA. ¹²Department of Ophthalmology, SUNY Downstate Medical Center, Brooklyn, New York, USA. ¹³Department of Radiology, Acibadem University School of Medicine, Istanbul, Turkey. ¹⁴Department of Radiology, Yale School of Medicine, New Haven, Connecticut, USA. ¹⁵Yale Center for Genome Analysis, Yale School of Medicine, New Haven, Connecticut, USA. ¹⁶Department of Molecular Biology and Genetics, Faculty of Science, Bilkent University, Ankara, Turkey. ¹⁷Howard Hughes Medical Institute, Yale School of Medicine, New Haven, Connecticut, USA. ¹⁸These authors contributed equally to this work. Correspondence should be addressed to M.G. (murat.gunel@yale.edu).

Received 24 January; accepted 21 April; published online 15 May 2011; doi:10.1038/ng.836

Figure 3 Species differences in expression of *LAMC3* in the cerebral cortex. (a) *In situ* hybridization of mid-fetal human brain (20 PCW) shows robust *LAMC3* expression in the cortical plate (CP) and within the germinal zones of the neocortical wall, including the ventricular zone (VZ) and subventricular zone (SVZ), and the outer SVZ (oSVZ). IZ, intermediate zone. (b) In contrast, *Lamc3* expression in the developing mouse brain (E13.5 to E17.5) is limited to the vasculature and meninges. (c) Human fetal neocortex (20 PCW) immunostained for *LAMC3* (green), the post-mitotic neuronal marker NeuN (red) and the neural stem cell marker SOX2 (blue) shows *LAMC3* to be strongly expressed in post-mitotic NeuN-positive neurons that have migrated and settled in the cortical plate (CP). Although *LAMC3* is not expressed in the intermediate zone, which contains migrating neurons, expression is seen in SOX2-positive neural stem cells in the ventricular zone and subventricular zone. In addition, *LAMC3* is expressed in the basal lamina of blood vessels. Composite images are shown on the right. See **Supplementary Figure 5** for individual panels.



staring and blinking spells (**Supplementary Note** and **Supplementary Video 3**). On her current examination at age 33 years, this subject was found to be neurologically intact with normal visual acuity and reportedly average intelligence. MRI revealed prominent bilateral smoothing and thickening of the lateral occipital cortex, which is associated with polymicrogyria (**Fig. 2b,c**, **Supplementary Fig. 3a** and **Supplementary Videos 4** and **5**). However, despite these gross structural findings, retinotopic mapping using functional MRI indicated that the relative locations and functions of the primary visual areas were largely indistinguishable from control subjects (**Fig. 2d**, **Supplementary Note** and **Supplementary Fig. 3b**)^{12,13}. Nonetheless, diffusion tensor imaging (DTI) tractography showed markedly lower fractional anisotropy and elevated radial diffusivity values in areas adjacent to the pachygyric region, suggesting microstructural changes of white matter, possibly caused by fiber disorganization (**Fig. 2e** and **Supplementary Note**).

Finally, we investigated the remaining affected individuals in our neurogenetics cohort of over 600 people to assess whether any had similar MRI findings. We identified only one other individual, NG 50-1, who had an almost identical MRI picture. This subject was the product of a second cousin marriage (**Fig. 2f**) and presented to medical attention at the age of 11 with episodes of vision loss consistent with seizures; imaging studies again revealed bilateral occipital pachygyria associated with polymicrogyria (**Fig. 2g**, **Supplementary Fig. 1b** and **Supplementary Note**). We found NG 50-1 to be heterozygous for the interval surrounding *LAMC3*, suggesting potential genetic locus heterogeneity (**Supplementary Table 5**). However, exome sequencing revealed no homozygous nonsense or frameshift mutations, whereas all eight new homozygous missense variants identified affected non-conserved domains of various proteins located within the autozygous intervals, suggesting that they were unlikely to be disease causing (**Supplementary Table 6**). Subsequent examination of the *LAMC3* sequence available from the exome sequencing data followed by confirmation using PCR and Sanger sequencing identified a compound heterozygous mutation, with a premature termination mutation at codon 386 (resulting in p.Gln386X) and a missense mutation (resulting in p.Gly350Arg) at a position completely conserved among vertebrate orthologs (**Supplementary Fig. 2c** and **Supplementary Fig. 4**) and predicted to be damaging. One mutation was inherited from each parent (**Supplementary Fig. 2c**).

None of the four mutations newly discovered in *LAMC3* had been previously reported in the dbSNP or 1000 Genomes databases and all were absent from our screening of 400 Turkish control subjects. They were also absent from our whole-exome sequence database

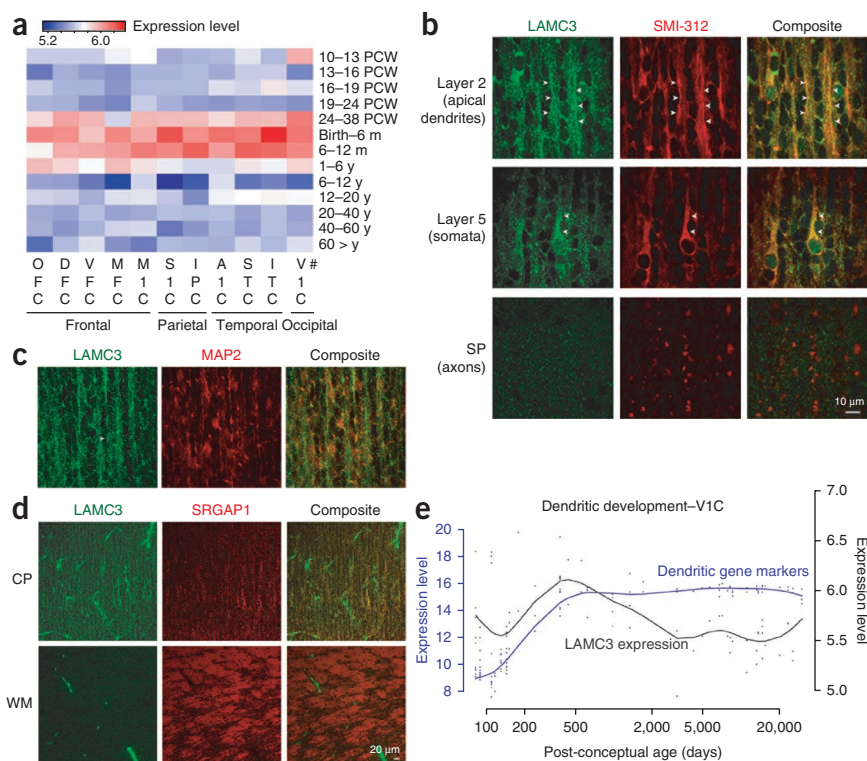
of 1,023 subjects with non-neurological diseases in which we only identified four different heterozygous *LAMC3* variants (p.Cys273Tyr, p.Gly275Glu, p.Gln928X and c.976+1G>A) with a collective allele frequency of less than 1 in 500, consistent with these deleterious alleles being under strong purifying selection. The rarity of such deleterious mutations and the finding of new homozygous and compound heterozygous mutations in *LAMC3* in all three subjects with occipital pachygyria and polymicrogyria provide conclusive evidence that recessive *LAMC3* mutations cause this syndrome.

We next investigated the expression of *LAMC3* in the developing human fetal brain at 20 post-conceptual weeks (PCW) and showed that it was enriched in the cortical plate, a dense layer of post-migratory pyramidal neurons, and was also present at lower levels in the ventricular and subventricular zones, the germinal layers of the cortex (**Fig. 3** and **Supplementary Fig. 5**). In contrast, we observed a strikingly different expression pattern in the embryonic mouse brain, where *Lamc3* expression was absent from the neuronal cells and was instead restricted to the embryonic cerebral vasculature and the meninges from embryonic day (E) 13.5 onwards (**Fig. 3b** and **Supplementary Fig. 6**). This finding, which is consistent with the previous observation that *Lamc3* deletion in mice is silent with no apparent phenotype¹⁴, suggested that *LAMC3* expression has diverged on the mammalian lineage, making the mouse a poor model for understanding *LAMC3* function in human cortical development.

We then investigated the spatial and temporal changes in expression during human cortical development and first detected *LAMC3* transcripts after mid-gestation, which peaked at an interval extending from late fetal development to late infancy (12 months) (**Fig. 4a**), coinciding with the period of cortical organization that takes place after neural stem cell proliferation and migration of postmitotic neurons to the cortical plate. Examination of *LAMC3* expression at the subcellular level supported these observations, showing that *LAMC3* primarily localizes to the soma and apical dendrite of pyramidal neurons (**Fig. 4b,c** and **Supplementary Fig. 7**) and is barely detected along or near the axons (**Fig. 4d**). A role for *LAMC3* in extracellular matrix organization of the somatodendritic compartment was further supported by an analysis of the Human Brain Transcriptome database¹⁵, showing that the developmental expression pattern of *LAMC3* parallels that of other molecules important for dendritogenesis (**Fig. 4e**)^{16,17} and synapse formation (**Supplementary Note**, **Supplementary Fig. 8** and **Supplementary Table 7**)¹⁸.

Laminins are extracellular cell adhesion molecules mostly localizing to basement membranes¹⁹ and are essential for early embryonic development. They are cross-shaped heterotrimers consisting of α , β

Figure 4 Temporal and spatial *LAMC3* expression pattern. **(a)** Heat map of *LAMC3* expression in human brain. The strongest expression was seen between late gestation (24–38 PCW) and late infancy (6–12 post-natal months) and is more prominent within the temporo-occipital lobes as compared to frontal regions. PCW, post-conceptual weeks; m, month; y, year. #Brain regions sampled are listed under Methods. **(b)** Human fetal neocortex (20 PCW) immunostained for *LAMC3* (green) and the neuronal marker SMI-312 (red) reveals high expression in pyramidal neurons in a punctate pattern primarily localizing to the somata and apical dendrites (arrowheads), both at the proximal and distal segments. *LAMC3* expression is not detected on axons as they leave the cortical plate (CP) and enter the subplate (SP). **(c)** In cortical layer 2, *LAMC3* (green) is localized to bundles of distal apical dendrites (arrowhead) immuno-positive for MAP2 (red), a marker for dendrites. **(d)** In the cortical plate, *LAMC3* (green) is expressed in pyramidal neurons. In the white matter (WM), where bundles of SRGAP1-positive corticofugal axons (red) are abundantly present, *LAMC3* is weak or absent on axons but highly expressed in the neighboring blood vessels. **(e)** *LAMC3* expression (black line) parallels that of genes known to be expressed during the period of dendritogenesis (blue line) within the V1 visual cortex (V1C) during late fetal and early post-natal periods and declines after infancy. For **a** and **e**, log₂-transformed expression values are shown (Online Methods).



and γ chains. Mutations in various laminin molecules lead to diverse pathologies including Pierson syndrome (congenital nephrotic syndrome with or without ocular abnormalities caused by *LAMB2* mutations), junctional epidermolysis bullosa ($\alpha 3$, $\beta 3$ and $\gamma 2$ chain mutations) and congenital merosin-deficient muscular dystrophy type 1A (*LAMA2* mutations), which is sometimes associated with cobblestone lissencephaly and occipital pachygyria^{19–21}. Mutations in *LAMC3* have not previously been reported. *LAMC3* is not thought to associate exclusively with the basement membrane—it can bind either to nidogen or to $\alpha 6\beta 1$ -integrin and is expressed in mouse retina and brain vessels^{22–25}, with *Lamc3* knockout mice lacking any overt phenotypes^{14,26}.

Little is known about the precise molecular mechanisms underlying human cortical gyration. Here we present conclusive genetic evidence that recessive *LAMC3* mutations cause human occipital cortical malformations characterized by complex gyration abnormalities and challenge the concept that cortical smoothing needs to be caused by disruption of early events in cortical neuronal migration exclusively. Further studies are needed to identify other molecules involved in the intricate process of cortical organization and to understand why the phenotype associated with *LAMC3* mutations is restricted to the occipital lobes.

URLs. dbSNP, <http://www.ncbi.nlm.nih.gov/projects/SNP/>; 1000 Genomes Project, <http://www.1000genomes.org/>; Human Brain Transcriptome database, <http://www.humanbraintranscriptome.org/>; RefSeq, <http://www.ncbi.nlm.nih.gov/RefSeq/>; DAVID Bioinformatics Resources, <http://david.abcc.ncifcrf.gov/>; Freesurfer, <http://surfer.nmr.mgh.harvard.edu/>; Java programming package, <http://billkent.edu/tr/~hboyaci/PsychWithJava/>; MedINRIA, <http://www-sop.inria.fr/asclepios/software/MedINRIA/index.php>.

METHODS

Methods and any associated references are available in the online version of the paper at <http://www.nature.com/naturegenetics/>.

Accession codes. *LAMC3* data are deposited in RefSeq under accession number NM_006059.

Note: Supplementary information is available on the Nature Genetics website.

ACKNOWLEDGMENTS

We are indebted to the subjects and families who have contributed to this study. We would like to thank M. State and J. Noonan for critical comments regarding the study and C. Camputaro for her help with the imaging studies. We acknowledge the use of Yale University Biomedical High Performance Computing Center for data analysis and storage. This study was supported by the Yale Program on Neurogenetics, the Yale Center for Human Genetics and Genomics, and US National Institutes of Health grants RC2NS070477 (to M.G.), UL1RR024139NIH (Yale Clinical and Translational Science Award) and UO1MH081896 (to N.S.). SNP genotyping was supported in part by a US National Institutes of Health Neuroscience Microarray Consortium award U24 NS051869-02S1 (to S.M.).

AUTHOR CONTRIBUTIONS

M.G. designed the study, and T.B., K.Y.K., A.L., R.P.L., N.S., K.B. and M.G. designed the experiments. T.B., K.Y.K., A.L., K.B., S.Y., M.B., A.O.C., A.K.O. and S.M. performed the experiments. V.D., S.S., B.T., H.K. and C.Y. identified, consented and recruited the study subjects and provided clinical information. A.D. and R.A.B. performed and evaluated magnetic resonance imaging. T.O., H.B., K.D. and E.A. performed and evaluated three-dimensional cortical reconstruction and functional imaging studies. M.C. and R.P.L. developed the bioinformatics scripts for data analysis. W.J.B. provided critical reagents. T.B., T.O., K.Y., K.B., R.P.L. and M.G. analyzed the genetics data. K.Y.K., A.L., Y.Z., N.S. and M.G. analyzed the expression data. T.B., K.Y.K., A.L., R.P.L., N.S., K.B. and M.G. wrote the paper.

COMPETING FINANCIAL INTERESTS

The authors declare competing financial interests: details accompany the full-text HTML version of the paper at <http://www.nature.com/naturegenetics/>.

Published online at <http://www.nature.com/naturegenetics/>.

Reprints and permissions information is available online at <http://npg.nature.com/reprintsandpermissions/>.

1. Rakic, P. Specification of cerebral cortical areas. *Science* **241**, 170–176 (1988).
2. Hofman, M.A. Size and shape of the cerebral cortex in mammals. I. The cortical surface. *Brain Behav. Evol.* **27**, 28–40 (1985).
3. Caviness, V.S. Jr. Mechanical model of brain convolitional development. *Science* **189**, 18–21 (1975).
4. Van Essen, D.C. A tension-based theory of morphogenesis and compact wiring in the central nervous system. *Nature* **385**, 313–318 (1997).
5. Kriegstein, A., Noctor, S. & Martinez-Cerdeno, V. Patterns of neural stem and progenitor cell division may underlie evolutionary cortical expansion. *Nat. Rev. Neurosci.* **7**, 883–890 (2006).
6. Piao, X. *et al.* G protein-coupled receptor-dependent development of human frontal cortex. *Science* **303**, 2033–2036 (2004).
7. Kostovic, I. & Rakic, P. Developmental history of the transient subplate zone in the visual and somatosensory cortex of the macaque monkey and human brain. *J. Comp. Neurol.* **297**, 441–470 (1990).
8. Ferrie, C.D., Jackson, G.D., Giannakodimos, S. & Panayiotopoulos, C.P. Posterior agyria-pachygyria with polymicrogyria: evidence for an inherited neuronal migration disorder. *Neurology* **45**, 150–153 (1995).
9. Ben Cheikh, B.O. *et al.* A locus for bilateral occipital polymicrogyria maps to chromosome 6q16–q22. *Neurogenetics* **10**, 35–42 (2009).
10. Barkovich, A.J., Kuzniecky, R.I., Jackson, G.D., Guerrini, R. & Dobyns, W.B. A developmental and genetic classification for malformations of cortical development. *Neurology* **65**, 1873–1887 (2005).
11. Bilgüvar, K. *et al.* Whole-exome sequencing identifies recessive *WDR62* mutations in severe brain malformations. *Nature* **467**, 207–210 (2010).
12. Sereno, M.I. *et al.* Borders of multiple visual areas in humans revealed by functional magnetic resonance imaging. *Science* **268**, 889–893 (1995).
13. Wandell, B.A., Dumoulin, S.O. & Brewer, A.A. Visual field maps in human cortex. *Neuron* **56**, 366–383 (2007).
14. Dénes, V. *et al.* Laminin deficits induce alterations in the development of dopaminergic neurons in the mouse retina. *Vis. Neurosci.* **24**, 549–562 (2007).
15. Johnson, M.B. *et al.* Functional and evolutionary insights into human brain development through global transcriptome analysis. *Neuron* **62**, 494–509 (2009).
16. Mrzljak, L., Uylings, H.B., Kostovic, I. & van Eden, C.G. Prenatal development of neurons in the human prefrontal cortex. II. A quantitative Golgi study. *J. Comp. Neurol.* **316**, 485–496 (1992).
17. Petanjek, Z., Judas, M., Kostovic, I. & Uylings, H.B. Lifespan alterations of basal dendritic trees of pyramidal neurons in the human prefrontal cortex: a layer-specific pattern. *Cereb. Cortex* **18**, 915–929 (2008).
18. Huttenlocher, P.R. & Dabholkar, A.S. Regional differences in synaptogenesis in human cerebral cortex. *J. Comp. Neurol.* **387**, 167–178 (1997).
19. Durbeej, M. Laminins. *Cell Tissue Res.* **339**, 259–268 (2010).
20. Helbling-Leclerc, A. *et al.* Mutations in the laminin alpha 2-chain gene (*LAMA2*) cause merosin-deficient congenital muscular dystrophy. *Nat. Genet.* **11**, 216–218 (1995).
21. Jones, K.J. *et al.* The expanding phenotype of laminin alpha2 chain (merosin) abnormalities: case series and review. *J. Med. Genet.* **38**, 649–657 (2001).
22. Gersdorff, N., Kohfeldt, E., Sasaki, T., Timpl, R. & Miosge, N. Laminin γ 3 chain binds to nidogen and is located in murine basement membranes. *J. Biol. Chem.* **280**, 22146–22153 (2005).
23. Koch, M. *et al.* Characterization and expression of the laminin γ 3 chain: a novel, non-basement membrane-associated, laminin chain. *J. Cell Biol.* **145**, 605–618 (1999).
24. Libby, R.T. *et al.* Laminin expression in adult and developing retinae: evidence of two novel CNS laminins. *J. Neurosci.* **20**, 6517–6528 (2000).
25. Yan, H.H. & Cheng, C.Y. Laminin α 3 forms a complex with β 3 and γ 3 chains that serves as the ligand for α 6 β 1-integrin at the apical ectoplasmic specialization in adult rat testes. *J. Biol. Chem.* **281**, 17286–17303 (2006).
26. Pinzón-Duarte, G., Daly, G., Li, Y.N., Koch, M. & Brunken, W.J. Defective formation of the inner limiting membrane in laminin α 2- and γ 3-null mice produces retinal dysplasia. *Invest. Ophthalmol. Vis. Sci.* **51**, 1773–1782 (2010).

ONLINE METHODS

Human subjects. The study protocol was approved by the Yale Human Investigation Committee (HIC) (protocol number 0908005592). Institutional review board approvals for genetic and MRI studies, along with written consent from all study subjects, were obtained by the referring physicians at the participating institutions. All fetal human tissues were collected under guidelines approved by the Yale HIC (protocol number 0605001466). Human fetal brains at 20 and 22 weeks of gestation were obtained from the Human Fetal Tissue Repository at the Albert Einstein College of Medicine (CCI number 1993-042).

Genome-wide genotyping. The Illumina Platform was used for genome-wide genotyping and analysis of the samples. Human 610K Quad BeadChips were used according to the manufacturer's protocol (Illumina).

Exome capture and sequencing. NimbleGen 2.1M human exome array version 1.0 (Roche Nimblegen, Inc.) was used to capture the exomes of samples NG 49-1 and NG 50-1 according to the manufacturer's protocol, with modifications^{11,27}. Sequencing of the library was performed on Genome Analyzer IIx using a single lane per subject (at a read length of 99 bp and 74 bp for NG 49-1 and NG 50-1, respectively) (Supplementary Table 2). The Illumina pipeline version 1.5 was used for image analysis and base calling.

Exome data analysis. Analysis of the sequencing data was performed according to the previously described data analysis pipeline we have developed^{11,27} by mapping the reads to the human genome (NCBI36/hg18) by Maq and BWA software^{28,29}. Coverage rates and distributions, as well as error positions and frequencies, were detected using perl scripts developed in house. Variants were called using SAMtools³⁰ and annotated for newness as compared to the dbSNP, Personal Genome and 1000 Genomes databases, as well as additional exome sequencing experiments we have performed. New variants were further evaluated for their impact on the encoded protein, conservation across 44 vertebrate species and *Caenorhabditis elegans* and *Drosophila melanogaster*, expression patterns and potential overlap with known miRNAs.

Sanger sequencing. Coding regions and exon-intron boundaries of *LAMC3* were evaluated by Sanger sequencing using standard protocols. Amplicons were cycle sequenced on ABI 9800 Fast Thermocyclers, and post cycle sequencing clean up was carried out with CleanSEQ System (Beckman Coulter Genomics). The amplicons were analyzed on 3730xL DNA Analyzer (Applied Biosystems Inc.).

Animals. All protocols performed in animal experiments were approved by the Institutional Animal Care and Use Committee at Yale School of Medicine. Embryonic day 0.5 was determined as the midday of the day of vaginal plug discovery. For embryonic stages, pregnant females were anesthetized, pups at appropriate stages were extracted from the uterus and the brains were dissected and fixed overnight by immersion in 4% paraformaldehyde in phosphate-buffered saline. Mouse brains were then cryoprotected in 30% sucrose in 4% paraformaldehyde and sectioned in the coronal plane on a Leica sledge cryomicrotome at 40 μ m (Leica Microsystems). Sections were mounted on slides and processed with *in situ* hybridization.

In situ hybridization. Sections were processed for non-radioactive *in situ* hybridization as described previously with minor modifications^{31,32}.

Immunofluorescence. Upon dissection, fetal human brains were immersed whole in 4% paraformaldehyde for 36 h, cryoprotected and frozen, and cryosectioned at 60 μ m. Standard techniques were used after primary antibodies were diluted in blocking solution containing normal donkey serum as follows: rabbit anti-LAMC3 (R96, W. Brunken, SUNY Downstate), 1:5,000; goat anti-SOX2 (Santa Cruz), 1:250; mouse anti-NeuN (Millipore), 1:1,000; mouse anti-SMI-312 (Covance), 1:250; mouse anti-MAP2 (Sigma), 1:1,000; and mouse anti-SRGA1 (Abcam), 1:250.

LAMC3 expression. The data were from a unique, high-quality microarray dataset that measured gene expression within different brain regions throughout human life using the Affymetrix Human Exon 1.0 ST arrays¹⁵ (see URLs).

The log₂-transformed expression values were calculated. The heat map was plotted by averaging the expression of *LAMC3* (*Laminin γ 3*) in the samples from the same cortical area and stage (Fig. 4a). The following cortical areas were sampled: orbital prefrontal cortex (OFC), dorsolateral prefrontal cortex (DFC), ventrolateral prefrontal cortex (VFC), medial prefrontal cortex (MFC), primary motor (M1) cortex (MIC), primary somatosensory (S1) cortex (S1C), posterior inferior parietal cortex (IPC), primary auditory (A1) cortex (A1C), posterior superior temporal cortex (STC), inferior temporal cortex (ITC) and primary visual (V1) cortex (V1C) (Fig. 4a).

To compare the relationship of *LAMC3* expression levels and developmental trajectories, functional gene lists for dendrite development (*MAP1A*, *MAPT* and *CAMK2A*) (Fig. 4e) and synaptogenesis (*SYP*, *SYPL1*, *SYPL2* and *SYN1*) (Supplementary Fig. 8) were manually curated. To summarize the principle gene expression profile of each category, principal component analysis was performed. The first principle component (PC1), which accounts for the majority of variability in the data, was plotted against age (to represent the developmental trajectory) and *LAMC3* expression level. The two independent datasets of synaptic density and the number of basal dendrites in the corresponding brain regions or areas were scaled by $\frac{x-\mu}{\sigma}$, in which μ and σ are the mean and the standard deviation of the values, respectively, corresponding to the time periods for which both our gene expression and the independently generated data were available. The scaled values were plotted against logarithmic age in days, and a cubic spline curve was fitted to display the developmental trajectories. The predicted values on this curve were calculated corresponding to available time points of previously generated independent data on dendrite development^{16,17} and synaptogenesis¹⁸. To identify developmentally co-expressed genes, we calculated the correlation of the temporal expression pattern of all other genes to that of *LAMC3*. The top 50 genes were selected for functional annotation, using DAVID Bioinformatics Resources 6.7 (see URLs)³³.

Primary human neuronal cell culture. All experiments were conducted in accordance with a protocol approved by the Yale Human Investigation Committee (principal investigator, N. Šestan, Protocol# 0605001466). Ventricular zone tissue was dissected from fetal human frontoparietal neocortical wall at 19 weeks of gestation, enzymatically dissociated and cultured in serum-free media in the presence of FGF-2 (20 ng/ml) and epidermal growth factor (20 ng/ml). After 4 weeks in culture, neural progenitor cells were transfected with a construct that co-expresses GFP and hemagglutinin (HA)-tagged human *LAMC3* (BC156274) using nucleofection (Lonza, kit VPG-1004; program A-033). One day after transfection, growth factors were withdrawn to facilitate neuronal differentiation. After 7 days in culture in the absence of growth factors, differentiated neurons were fixed and stained for GFP and HA.

MR data acquisition. MRI scanning was performed on a 3 Tesla scanner (Magnetom Trio, Siemens AG) with a twelve-channel phase-array head coil. A high-resolution T1-weighted three-dimensional anatomical-volume scan was acquired for each participant in the same session before the functional and DTI scans. BOLD signals in the functional scans were measured with an echo-planar imaging sequence. DTI data were acquired using a single-shot spin-echo echo-planar imaging sequence with parallel imaging technique GRAPPA.

MRI structural analysis procedures. Structural analysis involved three-dimensional reconstruction of the participants' cortices and computing cortical thickness using the Freesurfer analysis package (see URLs). After correction, the cortical thickness was calculated at each point as the shortest distance between the white matter-gray matter boundary and the gray matter-cerebrospinal fluid boundary. Finally, the cortical thickness measurement results were mapped on the three-dimensional model of the cortex using a color coding scheme for visualization.

Retinotopic mapping procedures. Experimental software for the retinotopic mapping fMRI scan was written by H.B. and K.D. in the Java programming platform (see URLs). In the scanner, the stimuli were back projected by a video projector fitted with a long throw lens onto a translucent back projection screen placed inside the scanner bore with the help of an angled first surface mirror. The functional scans were performed for retinotopic mapping following the methods developed by two previous studies^{34,12}.

Functional images were preprocessed by using the BrainVoyager QX software (Brain Innovation BI) and the three-dimensional model of the cortices were constructed and inflated for visualization. Functional images from all scans were spatially transformed and aligned with the anatomical volume obtained in the retinotopic mapping scan individually. Boundaries between retinotopic areas were drawn manually with a standard graphics program (Inkscape) after visual inspection of the cross-correlation maps of the BOLD response and the rotating wedges and of the BOLD response and the expanding annuli^{12,34}. The analysis of the second scan of NG 367-1 involved the same steps, except that instead of a cross-correlation analysis, we performed a general linear model analysis to identify the voxels that respond to vertical or horizontal wedges. We then visualized these voxels on the inflated cortex and used this as auxiliary information for manually drawing the boundaries between early visual areas.

DTI analysis procedures. White matter pathways were identified using the MRI Atlas of Human White Matter³⁵ and fiber tracking was performed in MedINRIA software package (see URLs). Fractional Anisotropy and Mean Diffusivity maps were computed in DTI studio³⁶ in three manually defined region of interest. Initial measurements are reported, and no further statistical analysis was performed.

27. Choi, M. *et al.* Genetic diagnosis by whole exome capture and massively parallel DNA sequencing. *Proc. Natl. Acad. Sci. USA* **106**, 19096–19101 (2009).
28. Li, H. & Durbin, R. Fast and accurate short read alignment with Burrows-Wheeler transform. *Bioinformatics* **25**, 1754–1760 (2009).
29. Li, H., Ruan, J. & Durbin, R. Mapping short DNA sequencing reads and calling variants using mapping quality scores. *Genome Res.* **18**, 1851–1858 (2008).
30. Li, H. *et al.* The Sequence Alignment/Map format and SAMtools. *Bioinformatics* **25**, 2078–2079 (2009).
31. Louvi, A., Sisodia, S.S. & Grove, E.A. Presenilin 1 in migration and morphogenesis in the central nervous system. *Development* **131**, 3093–3105 (2004).
32. Stillman, A.A. *et al.* Developmentally regulated and evolutionarily conserved expression of SLITRK1 in brain circuits implicated in Tourette syndrome. *J. Comp. Neurol.* **513**, 21–37 (2009).
33. Dennis, G. Jr. *et al.* DAVID: Database for Annotation, Visualization, and Integrated Discovery. *Genome Biol.* **4**, P3 (2003).
34. Engel, S.A., Glover, G.H. & Wandell, B.A. Retinotopic organization in human visual cortex and the spatial precision of functional MRI. *Cereb. Cortex* **7**, 181–192 (1997).
35. Song, S.K. *et al.* Demyelination revealed through MRI as increased radial (but unchanged axial) diffusion of water. *Neuroimage* **17**, 1429–1436 (2002).
36. Jiang, H., van Zijl, P.C., Kim, J., Pearlson, G.D. & Mori, S. DtiStudio: resource program for diffusion tensor computation and fiber bundle tracking. *Comput. Methods Programs Biomed.* **81**, 106–116 (2006).



Supplementary Material

for

Recessive *LAMC3* mutations cause malformations of occipital cortical development

Tanyeri Barak^{1,2,3,#}, Kenneth Y. Kwan^{2,4,#}, Angeliki Louvi^{1,2}, Veysi Demirbilek⁵, Serap Saygi⁶, Beyhan Tüysüz⁷, Murim Choi³, Hüseyin Boyacı^{8,9}, Katja Doerschner^{8,9}, Ying Zhu^{2,4}, Hande Kaymakçalan¹⁰, Saliha Yılmaz^{1,2,3}, Mehmet Bakırcıoğlu^{1,2,3}, Ahmet Okay Çağlayan^{1,2,3}, Ali Kemal Öztürk^{1,2,3}, Katsuhito Yasuno^{1,2,3}, William J. Brunken^{11,12}, Ergin Atalar⁹, Cengiz Yalçınkaya⁵, Alp Dinçer¹³, Richard A. Bronen^{1,14}, Shrikant Mane^{3,15}, Tayfun Özçelik¹⁶, Richard P. Lifton^{3,17}, Nenad Šestan^{2,4}, Kaya Bilgüvar^{1,2,3}, & Murat Günel^{1,2,3,*}

Departments of ¹Neurosurgery, ²Neurobiology and ³Genetics, Center for Human Genetics and Genomics and Program on Neurogenetics, Yale School of Medicine, New Haven CT, 06510, USA

⁴Kavli Institute for Neuroscience, Yale School of Medicine, New Haven, CT, 06510, USA

⁵Division of Child Neurology, Department of Neurology, Istanbul University Cerrahpasa Faculty of Medicine, Istanbul, 34098, Turkey

⁶Department of Neurology, Hacettepe University School of Medicine, Ankara, 06100, Turkey

⁷Division of Genetics, Department of Pediatrics, Istanbul University Cerrahpasa Faculty of Medicine, Istanbul, 34098, Turkey

⁸Department of Psychology and ⁹National Magnetic Resonance Research Center, Bilkent University, Ankara, 06800 Turkey

¹⁰Faculty of Arts and Sciences, Bahcesehir University, Istanbul, 34353, Turkey

Departments of ¹¹Cell Biology and ¹²Ophthalmology, SUNY Downstate Medical Center, Brooklyn, NY 11203

¹³Department of Radiology, Acibadem University School of Medicine, Istanbul, 34742, Turkey

¹⁴Department of Radiology, Yale School of Medicine, New Haven CT, 06510, USA

¹⁵Yale Center for Genome Analysis, Yale School of Medicine, New Haven, Connecticut 06510, USA

¹⁶Department of Molecular Biology and Genetics, Faculty of Science, Bilkent University, Ankara, 06800 Turkey

¹⁷Howard Hughes Medical Institute, Yale School of Medicine, New Haven, CT, 06510, USA

These authors contributed equally to the study

* To whom correspondence should be addressed (murat.gunel@yale.edu)

Supplementary Note

Functional MRI (fMRI)

Retinotopic mapping using fMRI indicated that the relative locations and functions of the primary visual areas in individual NG367-1 were largely indistinguishable from control subjects (**Fig. 2d** and **Supplementary Fig. 3b**). Specifically, in each hemisphere the foveal representation was mapped to the vicinity of the occipital pole; the primary visual cortex (striate cortex, V1) represented the full contralateral hemi-visual field and was flanked by dorsal and ventral parts of extrastriate visual areas (V2 and V3), with the former representing the lower quadrants of the visual contralateral hemifield and the latter corresponding to the upper quadrants.

Tractography results revealed the disorganization of short association fibers in the posterior part of the occipital lobe (**Fig. 2e**). We investigated white matter integrity in the pachygyric region by computing average fractional anisotropy (FA), mean diffusivity (MD) and radial diffusivity (RD) in manually defined regions of interest (ROIs) in the patient and two controls. We found markedly lower FA and elevated RD values in the patient in an ROI adjacent to the pachygyric region (patient: FA=0.32, sd=0.04, RD=6.88e-004 sd=2.6e-005; controls: FA=0.56, sd=0.04, RD=4.55e-004 sd=1.9e-005). Differences in mean diffusivity were not pronounced (patient: MD=8.4e-004, sd=4.1e-005, controls: MD=7e-004, sd=5.8e-005). These numbers suggest microstructural changes of white matter in the pachygyric region, possibly due to disorganization of fibers^{1,2}. No marked changes in FA, MD, or RD values were observed in the anterior or posterior parts of the inferior fronto-occipital pathway.

Co-expression profile of LAMC3 in human cortical development

To gain insight into the function of LAMC3 during human brain development, we analyzed functional annotations (false discovery rate (FDR) < 0.01) of the top 50 most highly co-expressed genes in the

Human Brain Transcriptome database (www.humanbraintranscriptome.org). We identified that the temporal and spatial expression pattern of several extracellular molecules, along with a known receptor for *LAMC3*, *nidogen 2*³, paralleled that of *LAMC3* (FDR = 4.0×10^{-10}) (**Supplementary Table 7**). The importance of the extracellular matrix has previously been shown not only for accurate structural organization but also for proper functioning of the cortex. For example, Reelin, an extracellular matrix protein that plays a fundamental role in neuronal cell migration during development is also important in cortical organization, including dendritogenesis and the formation of axonal projections, in the postnatal period^{4,5}. Our results suggest that *LAMC3* may function in occipital cortex development and organization in a similar manner.

Clinical Histories of Patients

NG 49-1

The patient is a 14 year-old left-handed girl born to a consanguineous union. She weighed 3 kg at birth (50th percentile), and no quantitative data is available for height and head circumference though these were noted to be normal. She presented to medical attention at age 2 with seizures typically involving loss of neck tone and consciousness. The frequency of the seizures increased over the next several years. On neurologic exam in 1999 at age 3, she had diminished visual acuity, mildly impaired abduction of the right eye, and delayed psychomotor development. Electroencephalogram (EEG) monitoring test revealed generalized slow spike waves, thought to be consistent with atypical absence seizures, which accompanied the forward drop of the head. Her seizures were ultimately controlled with valproic acid. During her last clinical visit within the past year, she was unable to read. She weighed 32 kg (10-25th percentile), was 1.43 m tall (25-50th percentile), and her head circumference was 50 cm (near 50th percentile). Her pre-existing strabismus had resolved, and musculoskeletal examination was within normal limits.

NG 367-1

The patient is a 33 year-old right-handed female who is the product of a first cousin consanguineous union. With the exception of a fall from approximately 2 meters at the age of 2.5, she had an uneventful neonatal and perinatal period, and reached mental and motor milestones on time. At the age of 10, she began experiencing seizures which consisted mostly of staring and blinking spells. At 14, she apparently experienced seizures during which she complained of an inability to see, though she later had no recollection of these episodes. The patient developed generalized tonic clonic (GTC) seizures at age 18. At age 21, she underwent a five-day inpatient scalp EEG monitoring during which she experienced four complex partial seizures with automatisms and forced blinking which localized to the bilateral posterior temporal/parieto-occipital lobes. Her epilepsy has been refractory to multiple trials of anti-epileptic medication but was finally controlled on a combination therapy that consisted of valproic acid, pregabalin, and topiramate. The longest seizure-free interval to date was four months. On her most recent medical visit, she was employed as an administrative assistant at a governmental office following her graduation from high school. On her neurological exam, her extraocular movements and vision were intact, and there was no nystagmus. The motor exam was grossly intact with normal strength and tone. No further work-up for muscular problems, which are associated with mutations in other laminin molecules, was performed. The rest of the neurological exam was unremarkable.

NG 50-1

The patient is a 16 year-old girl born to consanguineous parents. She weighed 2.75 kg at birth (10th percentile), height and head circumference were normal per report though these measurements are currently unavailable. She presented to medical attention at age 11. Her seizures, which were accompanied by autonomic symptoms, started at age 10. During video EEG monitoring, right parieto-occipital ictal activity was recorded and the patient experienced visual loss with head and eyes deviating

to the left side. During her last clinical visit this past year, she had normal ophthalmologic and musculoskeletal examinations. At this time, she weighed 41 kg (<3rd percentile), was 1.55 m tall (10th percentile), and her head circumference was 53 cm (50th percentile). The remainder of her physical examination was unremarkable.

Supplementary Videos

Supplementary Videos 1 and 2. Movies constructed from T2 axial (Video 1) and sagittal (Video 2) images (photographically inverted) of patient NG 49-1 demonstrate bilateral occipital pachgyria. The gray-white junction is ill-defined and there is thickening of both occipital cortices which appear smooth with loss of cerebral convolutions. Polymicrogyria is seen at the junction of the occipital and parietal lobes. The rest of the cerebrum, brainstem and cerebellum are grossly normal.

Supplementary Video 3. Audiovisual EEG monitoring of NG 367-1 revealed her typical complex partial seizure pattern with automatisms and forced blinking, which localizes to the bilateral posterior temporal/parieto-occipital lobes.

Supplementary Videos 4 and 5. Movies constructed from T2 axial (Video 3) and sagittal (Video 4) images of patient NG 367-1 (photographically inverted) shows a picture highly similar to that of NG 49-1 with smoothening and thickening of both occipital lobe cortices. Other cerebral lobes, the brainstem and cerebellum are grossly normal.

References

1. Song, S.K. et al. Dysmyelination revealed through MRI as increased radial (but unchanged axial) diffusion of water. *Neuroimage* **17**, 1429-36 (2002).
2. Mori, S. & Zhang, J. Principles of diffusion tensor imaging and its applications to basic neuroscience research. *Neuron* **51**, 527-39 (2006).
3. Gersdorff, N., Kohfeldt, E., Sasaki, T., Timpl, R. & Miosge, N. Laminin gamma3 chain binds to nidogen and is located in murine basement membranes. *J Biol Chem* **280**, 22146-53 (2005).
4. Tissir, F. & Goffinet, A.M. Reelin and brain development. *Nat Rev Neurosci* **4**, 496-505 (2003).
5. Frotscher, M. Role for Reelin in stabilizing cortical architecture. *Trends Neurosci* **33**, 407-14.

Supplementary Tables

Supplementary Table 1 | Homozygosity Intervals of Individual NG 49-1

Chromosome	Start	End	SNP Start	SNP End	Number of SNPs	Length (cM)*	Length (Mb)*
1	32,046,021	37,704,373	rs8179509	rs2245872	432	7.47	5.66
2	26,787	9,207,642	rs11900053	rs1467079	1079	19.77	9.18
2	191,611,003	202,543,473	rs3821236	rs10201429	690	8.71	10.93
3	9,168,324	14,566,350	rs2675186	rs9310449	624	9.68	5.40
8	40,291,664	43,910,848	rs2341978	rs10958798	219	2.83	3.62
8	47,062,007	61,889,433	rs7836486	rs10092214	1127	9.77	14.83
8	77,932,374	103,654,269	rs2733711	rs2511748	2344	21.78	25.72
9	12,275,170	27,620,562	rs10283912	rs12555345	2212	26.22	15.35
9	132,065,770	136,718,799	rs7028995	rs10776897	606	12.22	4.65
12	2,919,892	8,121,428	rs2302282	rs7132147	685	13.40	5.20
13	38,931,693	73,988,803	rs737645	rs1326711	3184	33.21	35.06
16	13,228,839	15,949,269	rs1898685	rs4148330	185	3.18	2.72
18	6,463,820	7,072,526	rs919093	rs8088532	103	2.70	0.61
20	48,802,413	52,652,385	rs1054185	rs1150423	480	8.58	3.85
X	2,710,157	6,155,942	rs5939319	rs2290487	227	5.61	3.45
X	22,817,873	35,484,817	rs5970937	rs5928914	1027	17.05	12.67
X	96,813,207	109,249,625	rs5966762	rs5942890	426	6.87	12.44
Total						209.06	171.32

* cM: centiMorgan, Mb: million base pair

Supplementary Table 2 | Coverage Distributions and Error Rates Across the Whole Exome and Homozygosity Intervals

Family ID		NG 49-1	NG 50-1
Number of lanes		1	1
Read Type (Single Read/Paired End)		PE	SR
Read length		99	74
Total number of reads (millions)		56.99	33.54
% mapped to the genome		95.28	98.78
Exome	% mapped to the exome	61.18	59.79
	Mean coverage	101.31	43.54
	% of bases covered at least 4X	97.52	94.81
	Mean error rate (%)	1.09	0.28
	2nd base error rate (%)	0.30	0.10
	Last base error rate (%)	4.70	0.82
Exomic Homozygosity Interval	Interval size (Mbs)	1.48	2.22
	% mapped to the interval	2.93	4.15
	Mean coverage	111.21	46.34
	% of bases covered at least 4X	98.70	95.91
	Mean error rate (%)	0.93	0.22
	2nd base error rate (%)	0.26	0.10
	Last base error rate (%)	4.12	0.70

Supplementary Table 3 | Sensitivity and Specificity for the Detection of Variants

SNP/Sample	NG 49-1		NG 50-1	
	Sensitivity ⁺	Specificity ⁺⁺	Sensitivity	Specificity
# of Het cSNPs by gt and seq*	1807		1785	
# of called Het cSNPs by seq		1810		1790
# of Het cSNPs by genotyping	1830		1865	
	98.74%	99.83%	95.71%	99.72%
# of Hom cSNPs by gt and seq	3948		3867	
# of called Hom cSNPs by seq		3962		3908
# of Hom cSNPs by genotyping	3965		3931	
	99.57%	99.65%	98.37%	98.95%

* Het: heterozygous, cSNP: coding SNP, gt: genotyping, seq: sequencing, Hom: homozygous

⁺ Sensitivity=# of cSNPs by gt and seq / # of cSNPs by genotyping

⁺⁺ Specificity= # of cSNPs by gt and seq / # of cSNPs by seq

Supplementary Table 4 | Novel Variants Identified within the Homozygosity Intervals of NG 49-1

Chr	Position	Base Change	Quality Score	Coverage	Non-reference Allele Coverage	Reference Allele Coverage	Gene	Status	Amino Acid Change	AminoAcid Position	PhyloP
9	132,901,464	-TG deletion	1054	34	28	1	LAMC3	Frame-shift	C301X	301/1575	-
9	135,331,228	T to C	255	114	57	0	SLC2A6	Missense	T172A	172/507	2.92
12	6,916,693	G to A	48	7	7	0	ATN1	Missense	G668R	668/1190	3.806
13	40,800,942	G to T	132	35	27	0	NARG1L	Missense	W258C	258/864	6.049
13	47,945,498	A to G	117	28	24	0	RB1	Missense	I831V	831/928	4.633
13	48,179,415	G to A	255	140	63	0	CYSLTR2	Missense	S154N	154/346	0.589
18	6,955,341	G to A	255	109	57	0	LAMA1	Missense	R2381C	2381/3075	3.932
X	2,846,140	G to A	255	83	83	0	ARSD	Missense	P190S	190/382	0.312
X	99,772,486	G to A	255	191	191	0	TSPAN6	Missense	R235C	235/245	2.093

Supplementary Table 5 | Homozygosity Intervals of Individual NG 50-1

Chromosome	Start	End	SNP Start	SNP End	Number of SNPs	Length (cM)*	Length (Mb)*
1	22,974,275	30,319,584	rs1561624	rs267667	559	7.60	7.35
2	37,949,126	46,343,636	rs2707237	rs2881321	917	10.55	8.39
2	174,634,997	204,770,878	rs1545361	rs6714929	2088	21.19	30.14
4	26,073,744	37,489,701	rs2788853	rs2995941	960	12.38	11.42
4	52,378,364	57,351,820	rs1910739	rs7681381	370	6.32	4.97
5	70,715,382	74,015,867	rs13168712	rs820870	334	5.09	3.30
6	16,744,783	22,919,946	rs909787	rs12211715	763	9.02	6.18
6	34,210,039	39,329,781	rs2499730	rs1744416	532	5.37	5.12
7	40,833,188	53,622,267	rs17688601	rs10488484	1251	14.97	12.79
10	90,977,544	95,352,040	rs2071510	rs3758538	399	4.64	4.37
10	97,974,301	116,262,976	rs1007764	rs2475233	1590	18.23	18.29
11	21,562,329	36,843,465	rs1945569	rs7107782	1282	17.41	15.28
13	45,249,732	57,720,052	rs3803195	rs4627212	997	9.56	12.47
13	96,346,535	101,270,253	rs7986491	rs10508076	572	7.57	4.92
15	66,712,579	75,771,535	rs8030733	rs4243047	583	7.96	9.06
20	49,707,586	51,400,261	rs2235858	rs6013667	200	3.26	1.69
X	9,763,544	23,701,445	rs2405940	rs5970795	1026	23.09	13.94
X	34,940,975	37,076,352	rs3124850	rs5917959	63	3.35	2.14
X	105,380,575	144,753,774	rs379742	rs6626452	2029	58.27	39.37
Total						245.83	211.19

* cM: centiMorgan, Mb: million base pair

Supplementary Table 6 | Novel Homozygous Variants Identified within the Homozygosity Intervals of NG 50-1

Chr	Position	Base Change	Quality Score	Coverage	Non-reference Allele Coverage	Reference Allele Coverage	Gene	Status	Amino Acid Change	Amino Acid Position	PhyloP
2	179,346,119	G to A	63	12	9	0	TTN	Missense	A2560V	2560/33423	5.118
6	20,591,060	A to G	255	82	45	0	E2F3	Missense	K272E	272/465	1.435
6	34,616,805	G to C	84	15	13	0	SPDEF	Missense	Q190E	190/335	3.451
15	73,441,049	G to C	51	8	7	0	MAN2C1	Missense	I389M	389/1040	4.397
X	12,849,410	C to A	244	73	39	1	TLR8	Missense	T777N	777/1041	1.155
X	19,465,763	C to T	150	37	25	0	SH3KBP1	Missense	R613Q	613/628	2.305
X	135,590,575	G to A	255	146	62	0	ARHGEF6	Missense	S562L	562/776	1.832
X	140,821,656	C to T	69	14	11	0	MAGEC1	Missense	S267F	267/1142	-1.143

Supplementary Table 7a | Top 150 genes with expression profiles that correlate with *LAMC3*

Rank	symbol	refseq	Cor to <i>LAMC3</i>	Rank	symbol	refseq	Cor to <i>LAMC3</i>
1	<i>LAMC3</i>	NM_006059	100.00%	41	<i>CYP1B1</i>	NM_000104	45.26%
2	<i>COL6A3</i>	NM_004369	56.58%	42	<i>EMCN</i>	NM_016242	45.17%
3	<i>COL18A1</i>	NM_130444	56.22%	43	<i>ENG</i>	NM_000118	45.12%
4	<i>IGF2</i>	NM_000612	56.17%	44	<i>C7</i>	NM_000587	44.92%
5	<i>IGF2</i>	NM_000612	55.30%	45	<i>LUM</i>	NM_002345	44.65%
6	<i>CXCL12</i>	NM_000609	54.80%	46	<i>TGFBI</i>	NM_000358	44.56%
7	<i>KANK2</i>	NM_015493	53.52%	47	<i>ASPN</i>	NM_017680	44.47%
8	<i>XPNPEP2</i>	NM_003399	52.98%	48	<i>ERG</i>	NM_001136154	44.43%
9	<i>COL6A2</i>	NM_001849	52.40%	49	<i>PDE4C</i>	NM_000923	44.39%
10	<i>COL3A1</i>	NM_000090	51.66%	50	<i>MXRA5</i>	NM_015419	44.38%
11	<i>COL15A1</i>	NM_001855	51.46%	51	<i>FGD5</i>	NM_152536	44.32%
12	<i>COL1A1</i>	NM_000088	50.68%	52	<i>ALPK3</i>	NM_020778	44.25%
13	<i>CD248</i>	NM_020404	50.57%	53	<i>FN1</i>	NM_212482	44.16%
14	<i>ITIH2</i>	NM_002216	50.38%	54	<i>CPZ</i>	NM_001014448	44.08%
15	<i>CCND1</i>	NM_053056	50.22%	55	<i>CRYAA</i>	NM_000394	43.91%
16	<i>DOCK6</i>	NM_020812	49.50%	56	<i>FGF8</i>	NM_033163	43.79%
17	<i>FLI1</i>	NM_002017	49.47%	57	<i>RHBDF1</i>	NM_022450	43.69%
18	<i>SRPX2</i>	NM_014467	48.15%	58	<i>IGFBP4</i>	NM_001552	43.59%
19	<i>COL1A2</i>	NM_000089	47.56%	59	<i>MPZL2</i>	NM_144765	43.51%
20	<i>ANPEP</i>	NM_001150	47.52%	60	<i>ARHGEF15</i>	NM_173728	43.42%
21	<i>GATA6</i>	NM_005257	47.44%	61	<i>OGN</i>	NM_033014	43.32%
22	<i>CETP</i>	NM_000078	47.01%	62	<i>CYSLTR1</i>	NM_006639	43.30%
23	<i>EDN3</i>	NM_207032	46.94%	63	<i>COLEC12</i>	NM_130386	43.11%
24	<i>CD28</i>	NM_006139	46.83%	64	<i>ST14</i>	NM_021978	43.01%
25	<i>ALDH1A2</i>	NM_003888	46.73%	65	<i>SLC6A2</i>	NM_001043	42.95%
26	<i>LYVE1</i>	NM_006691	46.62%	66	<i>TJP3</i>	NM_014428	42.80%
27	<i>MMRN2</i>	NM_024756	46.55%	67	<i>BARX2</i>	NM_003658	42.72%
28	<i>ATP2A1</i>	NM_004320	46.51%	68	<i>DAB2</i>	NM_001343	42.61%
29	<i>DSP</i>	NM_004415	46.39%	69	<i>ITGA5</i>	NM_002205	42.58%
30	<i>SIGLEC1</i>	NM_023068	46.06%	70	<i>FAM83C</i>	NM_178468	42.39%
31	<i>CDH5</i>	NM_001795	46.06%	71	<i>ATP8B3</i>	NM_138813	42.38%
32	<i>CD209</i>	NR_026692	45.87%	72	<i>STARD8</i>	NM_001142503	42.35%
33	<i>BGN</i>	NM_001711	45.67%	73	<i>HOXB3</i>	NM_002146	42.35%
34	<i>LSR</i>	NM_205834	45.52%	74	<i>PCOLCE</i>	NM_002593	42.20%
35	<i>ADCY4</i>	NM_139247	45.52%	75	<i>MALL</i>	NM_005434	42.02%
36	<i>OLFML2A</i>	NM_182487	45.50%	76	<i>ELN</i>	NM_000501	42.00%
37	<i>FMOD</i>	NM_002023	45.45%	77	<i>ETS1</i>	NM_001143820	41.98%
38	<i>NID2</i>	NM_007361	45.40%	78	<i>GJA5</i>	NM_005266	41.97%
39	<i>STAB1</i>	NM_015136	45.36%	79	<i>WFIKK2</i>	NM_175575	41.96%
40	<i>SLC6A20</i>	NM_020208	45.32%	80	<i>FAM83E</i>	NM_017708	41.87%

Rank	symbol	refseq	Cor to LAMC3	Rank	symbol	refseq	Cor to LAMC3
81	<i>PRND</i>	NM_012409	41.81%	116	<i>SLC22A8</i>	NM_004254	39.78%
82	<i>EFCAB4B</i>	NM_001144958	41.64%	117	<i>LAMA2</i>	NM_000426	39.71%
83	<i>AOC3</i>	NM_003734	41.40%	118	<i>VASN</i>	NM_138440	39.61%
84	<i>HRC</i>	NM_002152	41.35%	119	<i>LOXL2</i>	NM_002318	39.60%
85	<i>C21orf93</i>	AF427488	41.33%	120	<i>KLF4</i>	NM_004235	39.58%
86	<i>FAM83F</i>	NM_138435	41.30%	121	<i>AMHR2</i>	NM_020547	39.51%
87	<i>PLAU</i>	NM_002658	41.22%	122	<i>ITGA11</i>	NM_001004439	39.50%
88	<i>PRM3</i>	NM_021247	41.21%	123	<i>BNC2</i>	NM_017637	39.49%
89	<i>ACTG2</i>	NM_001615	41.15%	124	<i>CD7</i>	NM_006137	39.42%
90	<i>ABCC3</i>	NM_003786	41.14%	125	<i>SCGB1A1</i>	NM_003357	39.33%
91	<i>NPR1</i>	NM_000906	40.95%	126	<i>STRA6</i>	NM_022369	39.32%
92	<i>MIOX</i>	NM_017584	40.94%	127	<i>ACR</i>	NM_001097	39.24%
93	<i>OTOP3</i>	NM_178233	40.92%	128	<i>WNK4</i>	NM_032387	39.13%
94	<i>BMP6</i>	NM_001718	40.91%	129	<i>CLEC1A</i>	NM_016511	39.13%
95	<i>PSTPIP1</i>	NM_003978	40.90%	130	<i>C20orf144</i>	DQ080434	39.12%
96	<i>BMP5</i>	NM_021073	40.89%	131	<i>CTGF</i>	NM_001901	39.12%
97	<i>NMUR2</i>	NM_020167	40.89%	132	<i>NID1</i>	NM_002508	39.06%
98	<i>KANK3</i>	NM_198471	40.83%	133	<i>HIC1</i>	NM_001098202	39.06%
99	<i>PLEKHA4</i>	NM_020904	40.81%	134	<i>AEN</i>	NM_022767	39.03%
100	<i>OR51E1</i>	NM_152430	40.58%	135	<i>CYP1A2</i>	NM_000761	39.01%
101	<i>RBP5</i>	NM_031491	40.49%	136	<i>OLFML1</i>	NM_198474	38.98%
102	<i>CTSL2</i>	NM_001333	40.47%	137	<i>ZNF761</i>	NM_001008401	38.98%
103	<i>P2RX1</i>	NM_002558	40.46%	138	<i>GPR124</i>	NM_032777	38.95%
104	<i>ADAMTS12</i>	NM_030955	40.42%	139	<i>CREB3L1</i>	NM_052854	38.95%
105	<i>COL20A1</i>	NM_020882	40.33%	140	<i>MYLK2</i>	NM_033118	38.94%
106	<i>MYO18B</i>	NM_032608	40.17%	141	<i>APOA5</i>	NM_052968	38.87%
107	<i>ESRP2</i>	NM_024939	40.15%	142	<i>OR10G4</i>	NM_001004462	38.84%
108	<i>TMC4</i>	NM_001145303	40.09%	143	<i>C21orf125</i>	NR_026960	38.82%
109	<i>KRTAP5-3</i>	NM_001012708	40.08%	144	<i>GPR97</i>	NM_170776	38.81%
110	<i>PLVAP</i>	NM_031310	40.06%	145	<i>DSG3</i>	NM_001944	38.75%
111	<i>HOXC8</i>	NM_022658	40.04%	146	<i>KRT38</i>	NM_006771	38.72%
112	<i>SLC6A13</i>	NM_016615	39.99%	147	<i>OLFML2B</i>	NM_015441	38.71%
113	<i>KDEL3</i>	NM_006855	39.89%	148	<i>UPK1A</i>	NM_007000	38.69%
114	<i>CALCA</i>	NM_001741	39.83%	149	<i>DRD4</i>	NM_000797	38.69%
115	<i>MYH6</i>	NM_002471	39.83%	150	<i>MYBPC2</i>	NM_004533	38.67%

Supplementary Table 7b | GO Pathway genes with expression profiles that correlate with *LAMC3* (analysis based on top 50 genes)

GO:0031012~extracellular matrix (False discovery rate (FDR) = 4.0×10^{-10})

COL18A1, ASPN, FMOD, CD248, LUM, COL3A1, COL15A1, OLFML2A, NID2, MMRN2, BGN, TGFBI, COL6A3, COL1A2, COL6A2, COL1A1

GO:0044421~extracellular region part (FDR = 1.7×10^{-9})

COL18A1, ASPN, FMOD, EDN3, LUM, CD248, COL3A1, COL15A1, OLFML2A, IGF2, NID2, LSR, CXCL12, MMRN2, BGN, TGFBI, COL6A3, COL1A2, COL6A2, CETP, COL1A1, ENG

GO:0005576~extracellular region (FDR = 2.6×10^{-9})

ASPN, FMOD, C7, EDN3, EMCN, CD248, LUM, COL3A1, LSR, CXCL12, MMRN2, TGFBI, COL6A3, COL6A2, ITIH2, CETP, COL18A1, COL15A1, OLFML2A, IGF2, NID2, MXRA5, SIGLEC1, BGN, SRPX2, CD209, COL1A2, COL1A1, ENG

GO:0005578~proteinaceous extracellular matrix (FDR = 3.1×10^{-9})

COL18A1, ASPN, FMOD, CD248, LUM, COL3A1, COL15A1, NID2, MMRN2, BGN, TGFBI, COL6A3, COL1A2, COL6A2, COL1A1

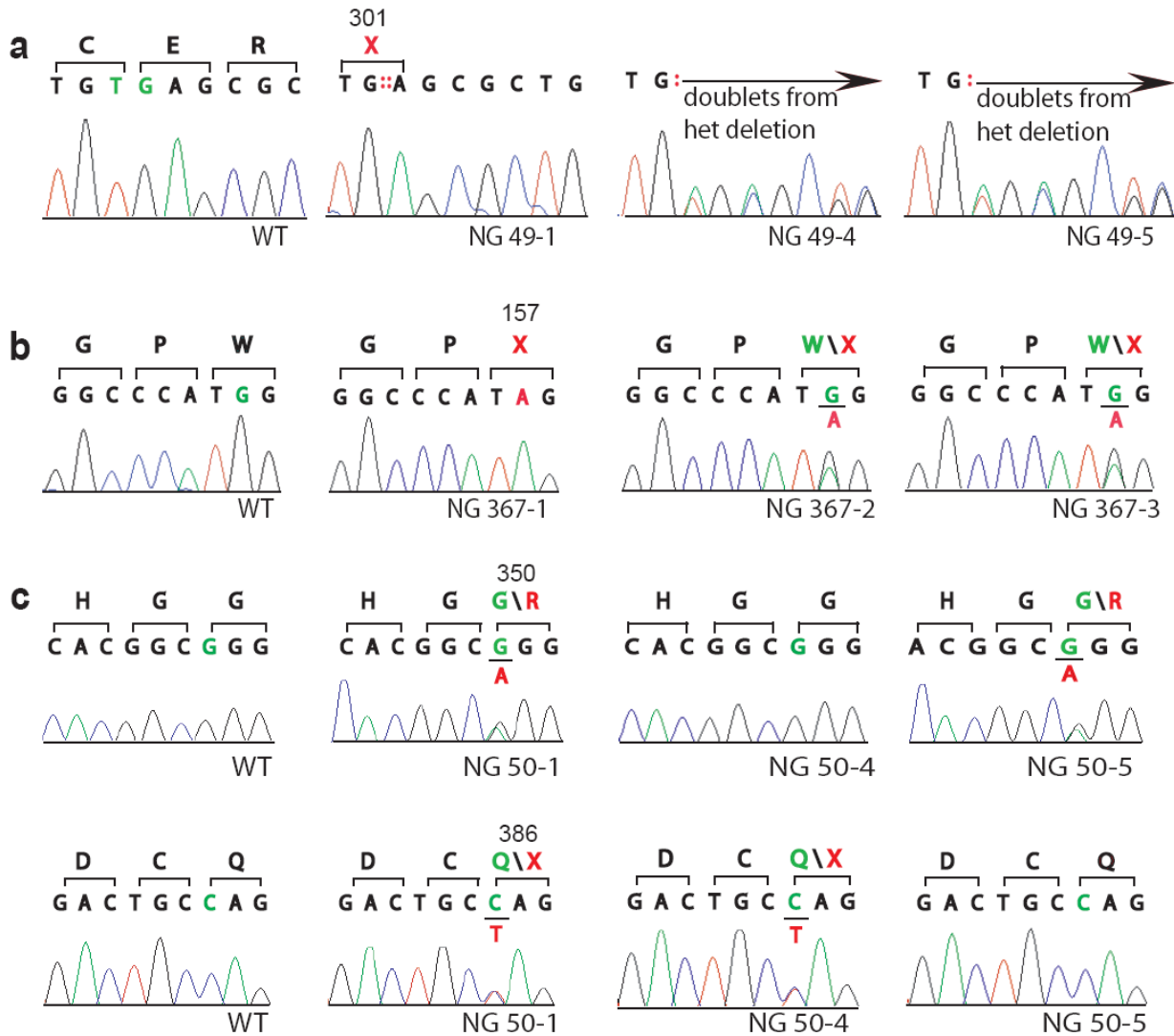
GO:0030198~extracellular matrix organization (FDR = 9.2×10^{-7})

COL18A1, LUM, TGFBI, COL3A1, COL1A2, COL6A2, OLFML2A, COL1A1, ENG

Supplementary Figures

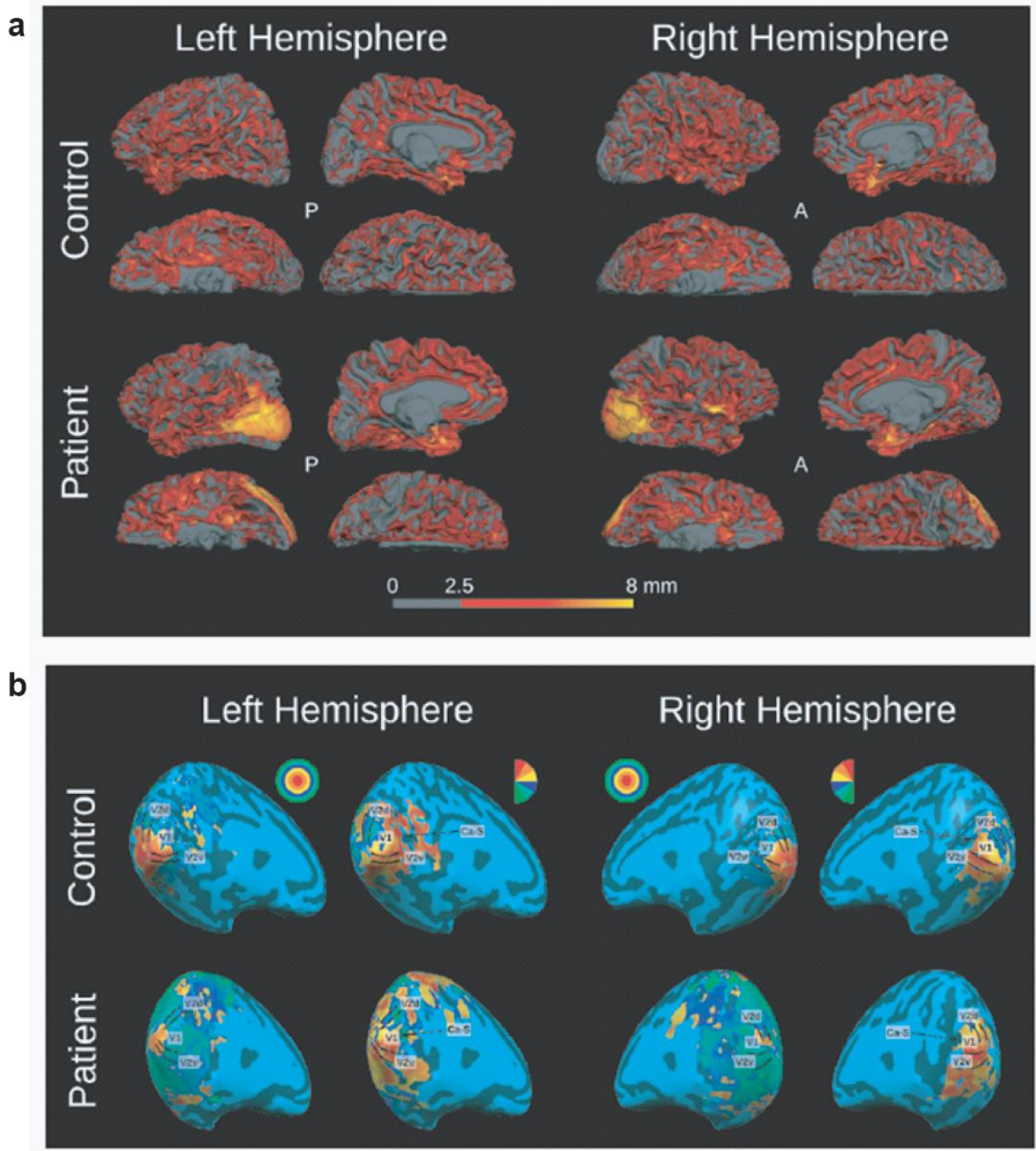


Supplementary Figure 1 | Clinical images of patients NG 49-1 (a) and NG 50-1 (b). Pictures of patients are published with written informed consent from their parents.



Supplementary Figure 2 | Sequence traces of wild type along with the three index cases and their parents.

From left to right, the panels show the sequence traces in a control subject, the patients and the patients' parents, respectively. The predicted amino acids corresponding to each codon are represented above the nucleotide sequences which are marked in bold letters above the chromatograms. For each sequence, the mutated base(s) are shown in red, as are resultant amino acid substitutions. For the wild type sequences, the altered bases are shown in green. Note that all patients are homozygous for the mutations whereas both parents are heterozygous. The following mutations are observed: (a) NG 49-1: p.Cys301X, (b) NG 367-1: p.Trp157X, (c) NG 50-1: p.Gly350Arg, p.Gln386X; NG 50-5: p.Gly350Arg and NG 50-4: p.Gln386X.



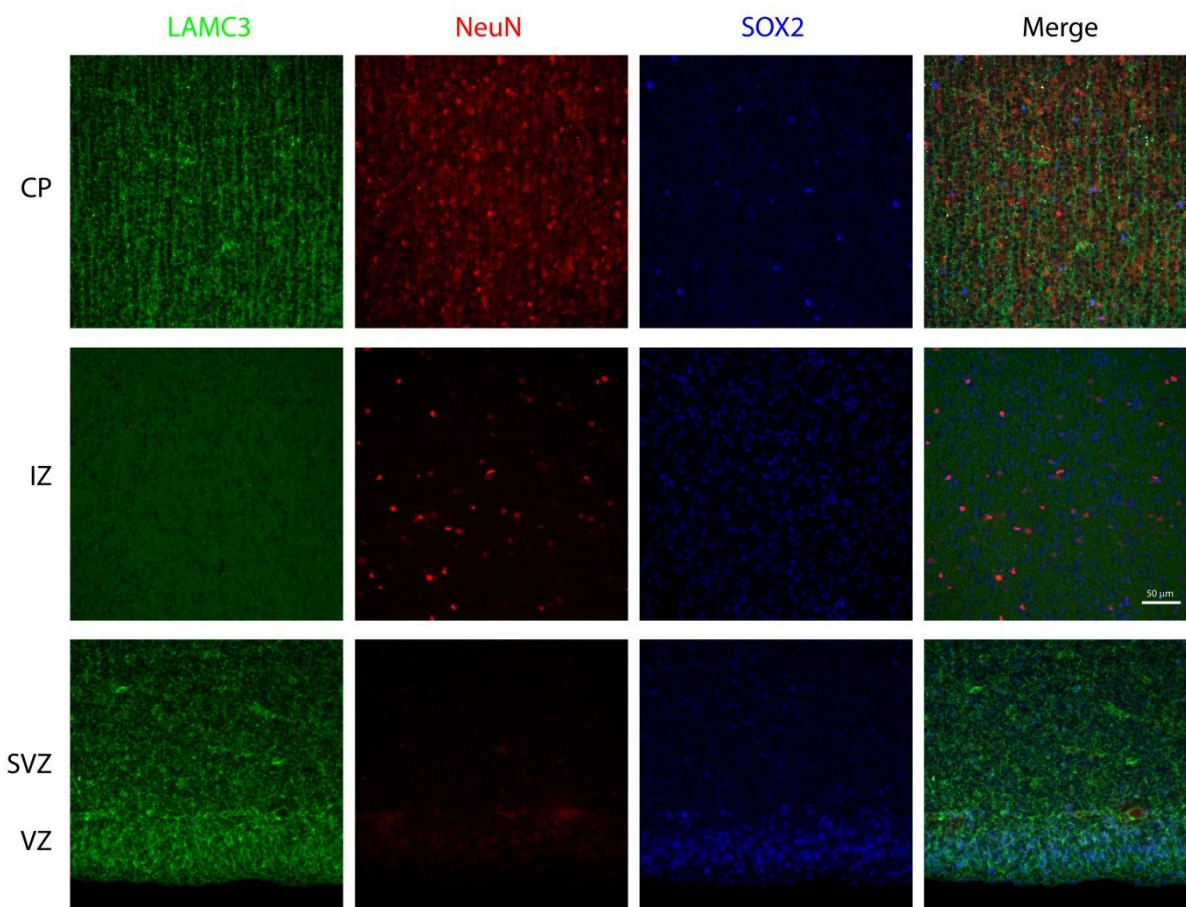
Supplementary Figure 3 | Functional MRI studies (a) Three dimensional reformatting of MR images shows the lateral occipital cortex to be significantly thickened in NG 367-1 as compared to a control subject in which the cortex is normal in thickness. A bar representing the color coding for the cortical thickness is shown.

A:anterior, P: posterior.

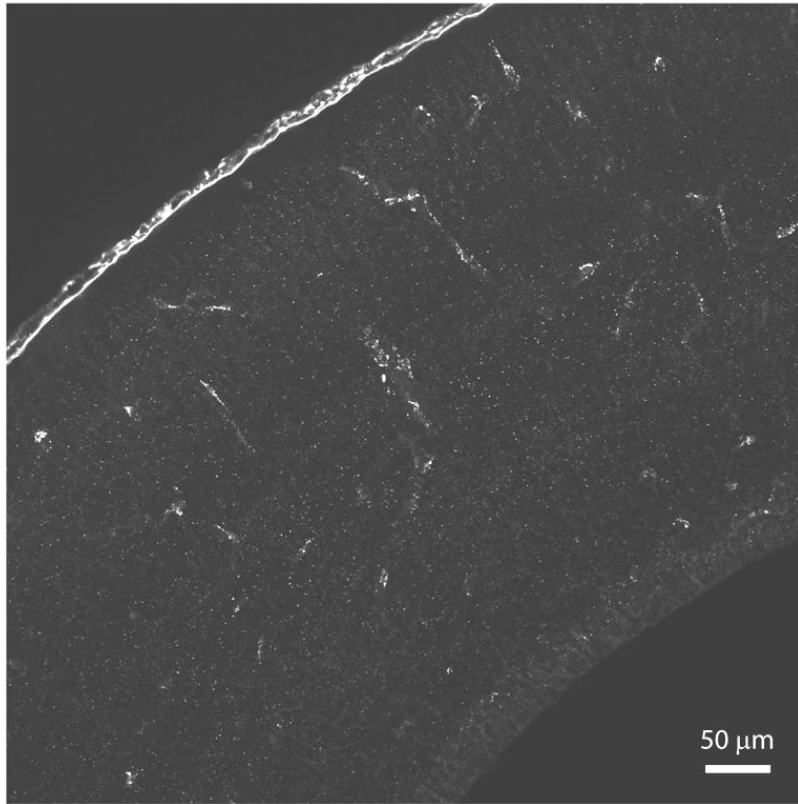
(b) The retinotopic mapping in subject NG 367-1 reveals that the anatomical locations of the primary visual areas and the spatial patterns of their activity in response to visual stimulation in NG 367-1 are similar to control subjects. The stimuli presented are shown on top.



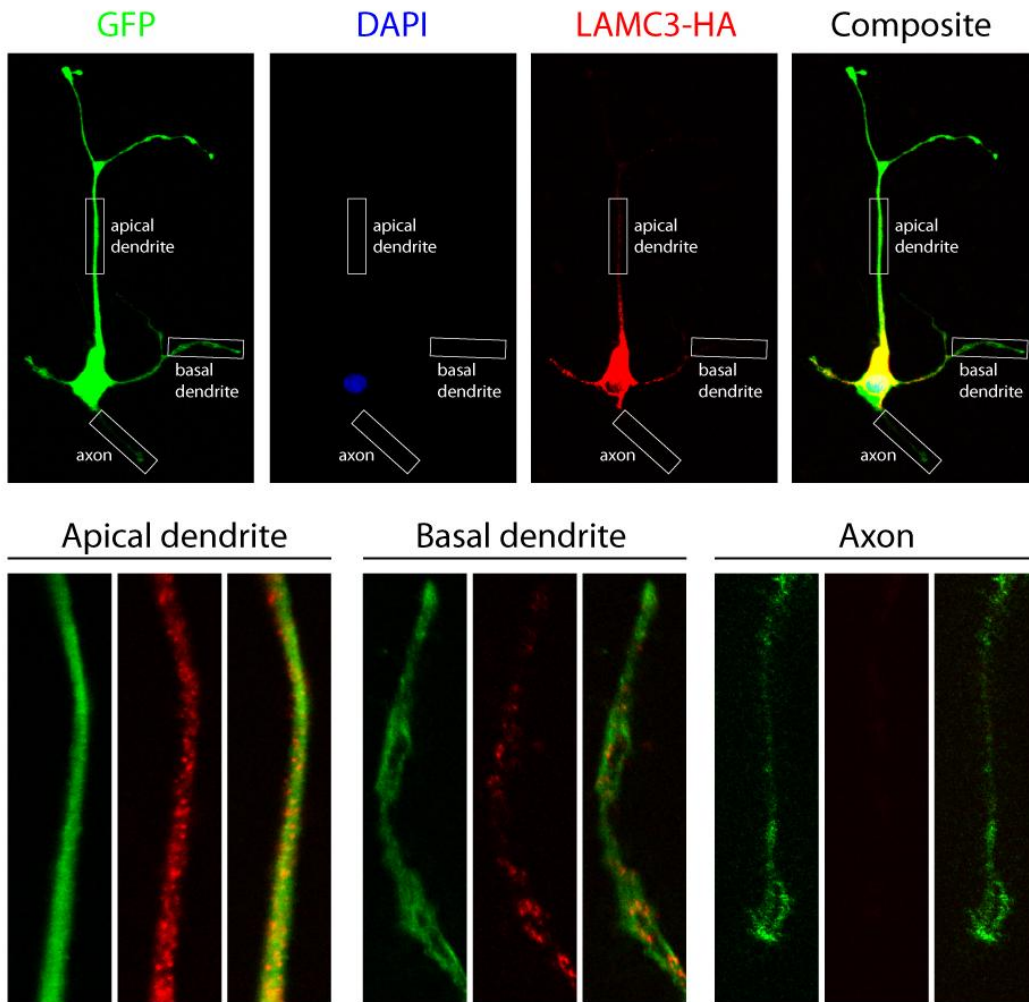
Supplementary Figure 4 | p.Gly350Arg mutation in individual NG 50-1. The glycine residue is completely conserved across 44 species, suggesting that the p.Gly350Arg mutation is likely to be damaging.



Supplementary Figure 5 | LAMC3 is expressed in the cortical plate and the germinal zones of the fetal human neocortical wall. Human fetal neocortex at 20 post-conceptual weeks was immunostained for LAMC3 (green), the post-mitotic neuronal marker NeuN (red), and the neural stem cell marker SOX2 (blue). LAMC3 is strongly expressed in post-mitotic NeuN-positive neurons that have migrated and settled in the cortical plate (CP). LAMC3 is not expressed in the intermediate zone (IZ), which contains migrating neurons. LAMC3 is expressed in SOX2-positive neural stem cells in the ventricular zone (VZ) and subventricular zone (SVZ). In addition, LAMC3 is expressed in the basal lamina of blood vessels.

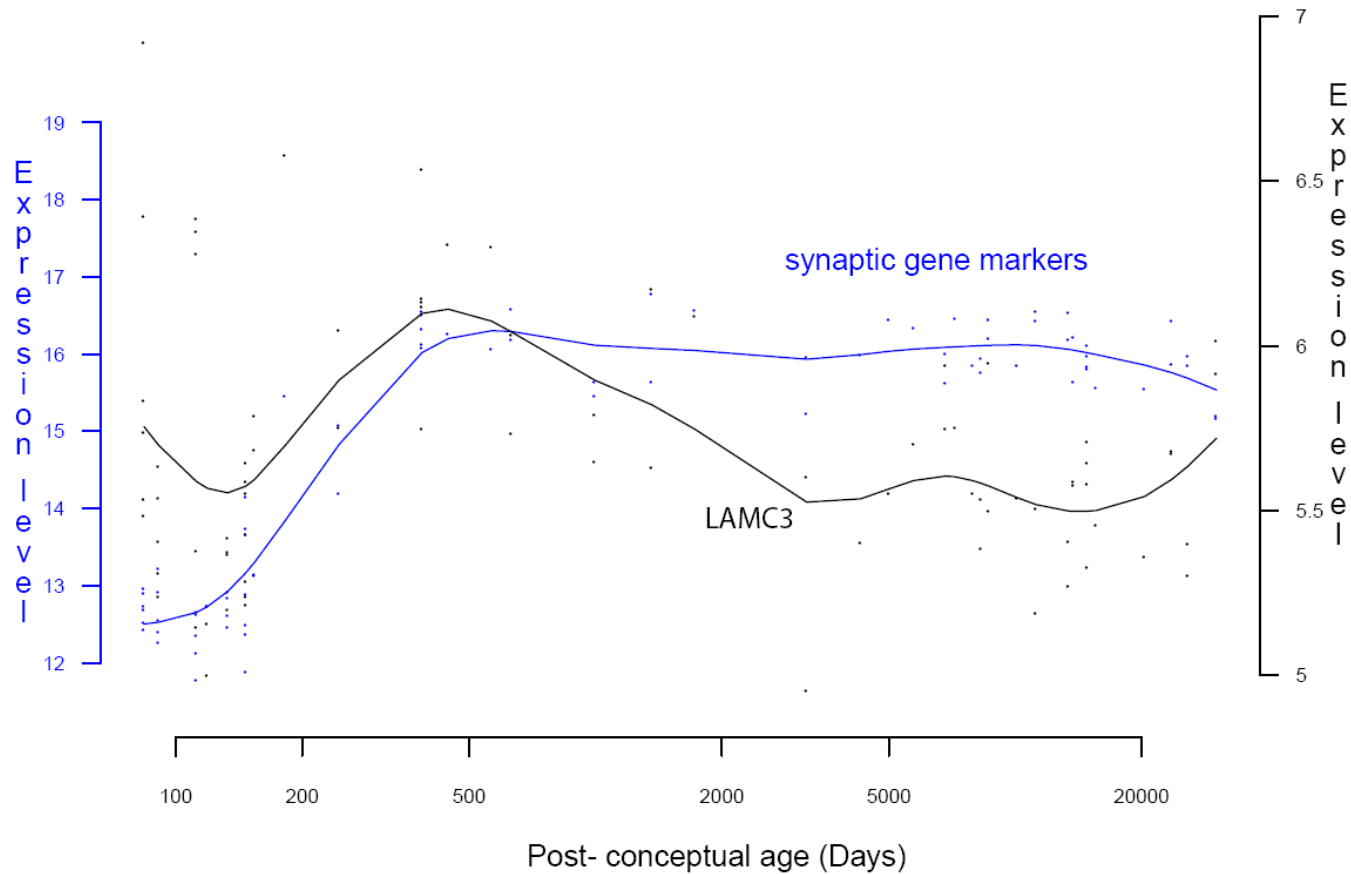


Supplementary Figure 6 | LAMC3 is absent from neural progenitors and neurons in the embryonic day 17.5 mouse cortical wall. Mouse neocortex at embryonic day (E) 17.5 was immunostained for LAMC3. LAMC3 was present in the basal lamina of blood vessels and meninges but absent from the cortical germinal zones, which contain neural progenitors, and the cortical plate, which contain post-mitotic neurons.



Supplementary Figure 7 | LAMC3 localizes primarily to the somatodendritic compartment in cultured fetal human primary neuronal cells. Neural progenitor cells were isolated from fetal human neocortex at 17 post-conceptual weeks and expanded in vitro in the presence of growth factors. After 4 weeks in culture, progenitor cells were transfected with a construct that co-expresses GFP and HA-tagged human LAMC3 using nucleofection. One day after transfection, growth factors were withdrawn to facilitate neuronal differentiation. Neurons were fixed 7 days after growth factor withdrawal and stained for GFP and HA. Tagged human LAMC3 predominantly localizes to the soma, both the apical and basal dendrites, but is mostly absent from the axon. These results are consistent with our immunolocalization of LAMC3 in the intact human fetal neocortex.

Synaptogenesis-V1C



Supplementary Figure 8 | *LAMC3* expression (black line) parallels that of genes that mark synaptogenesis (*SYP*, *SYPL1*, *SYPL2*, *SYN1*, blue line) within the V1 visual cortex (V1C) during a period between late gestation to late infancy. log 2 of the first principle component (PC1), which accounts for the majority of variability of the expression data (see **Methods**), was plotted against age to represent the developmental trajectory. log2 of *LAMC3* expression is shown on the right vertical axis.